ACS SENSORS

pubs.acs.org/acssensors

Article

Redox Cycling Amplified Electrochemical Lateral-Flow Immunoassay: Toward Decentralized Sensitive Insulin Detection

Ponnusamy Nandhakumar,[§] Cristina Muñoz San Martín,[§] Beatriz Arévalo,[§] Shichao Ding,[§] Mahika Lunker, Eva Vargas, Omeed Djassemi, Susana Campuzano, and Joseph Wang*

Cite This: *ACS Sens.* 2023, 8, 3892−3901

Read Online

ACCESS | Metrics & More | Article Recommendations | Supporting Information

ABSTRACT: While paper-based lateral-flow immunoassays (LFA) offer considerable promise for centralized diagnostic applications, the analytical capability of conventional LFA remains constrained due to the low sensitivity of its common optical detection strategy. To address these issues, we report a simple electrochemical LFA (eLFA) with nanocatalytic redox cycling for decentralized insulin detection. Simultaneous binding of insulin with detection antibodies and capture antibodies through the capillary flow at the LFA platform and signal amplification through the rapid nanocatalytic reduction of $[Fe(CN)_6]^{3-}$ (Fe^{3+}) with Au nanoparticles (AuNP) and ammonia-borane (AB), coupled to electrochemical redox cycling reactions involving Fe^{3+}, AuNP, and AB on the carbon working electrode, offer higher sensitivity than conventional colorimetric LFA and enzymatic redox cycling. The resulting integrated eLFA strip allows the detection of low insulin concentrations (LOD = 12 pM) and offers considerable promise for highly sensitive decentralized assays of different biological fluids (saliva and serum) without additional pretreatment or washing steps.

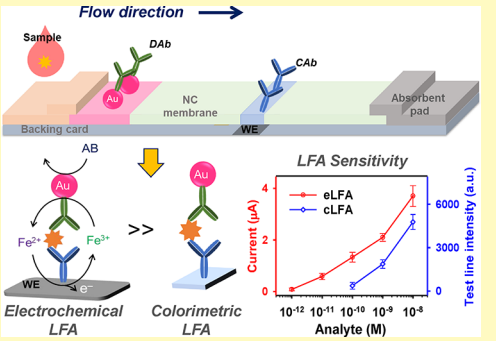

KEYWORDS: *Lateral-flow immunoassay, eLFA, immunosensor,, nanocatalytic redox cycling, diabetes mellitus, insulin detection, point-of-care testing*

Paper-based lateral flow immunoassays (LFAs) have emerged as a prominent diagnostic tool due to their simplicity, cost-effectiveness, and rapid results.[1−3] LFAs are commonly used for the detection of various analytes, including infectious disease biomarkers and hormones. Traditionally, LFAs have relied on optical detection strategies, utilizing colorimetric or fluorescent labels to provide qualitative or semiquantitative results,[4−7] depending on the visual interpretation of test line intensity or the use of specialized readers to quantify the signal. Colorimetric-based LFAs (cLFA) utilize colored particles, such as gold nanoparticles, colloidal dyes, or quantum dots, which produce visible color changes upon target binding. Although cLFAs are simple and cost-effective, they suffer from limitations in their sensitivity and quantification. The detection of low-abundance analytes in a complex matrix (e.g., whole blood) is especially lacking with this detection strategy. On the other hand, fluorescence-based LFAs employ fluorescent tags that emit a signal when excited by an appropriate light source.[8] While fluorescence offers enhanced sensitivity and quantification compared to colorimetry, it requires specialized equipment for excitation and detection, making it less suitable for POC applications. However, with the increasing demand for portable and user-friendly devices, electrochemical LFAs (eLFA) have gained considerable recent attention.[9−11] The eLFA is not only simple to use, portable, and rapid to detect various analytes but also offers good sensitivity, accuracy, and selectivity when compared to optical LFA. The integration of electrochemical techniques into LFAs offers several advantages, such as enhanced sensitivity, quantitative measurements, and the potential for miniaturization and integration with point-of-care (POC) platforms. Moreover, the use of electrode-based conversion to transmit electrical signals in eLFA makes it easy to integrate with miniaturized potentiostats that are compatible with smartphones and portable analyzers.

Here, we report a redox-cycling-combined simple eLFA strip for detecting trace insulin in human serum and saliva. The detection of insulin holds significant clinical relevance, considering its pivotal role in regulating glucose metabolism and its association with diabetes mellitus.[12−16] Timely and accurate measurement of insulin levels in decentralized settings is crucial for effective diabetes management, enabling healthcare professionals to optimize therapeutic strategies toward optimal glycemic control. Conventional laboratory-based

Received: July 14, 2023
Accepted: September 8, 2023
Published: September 21, 2023

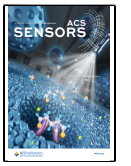

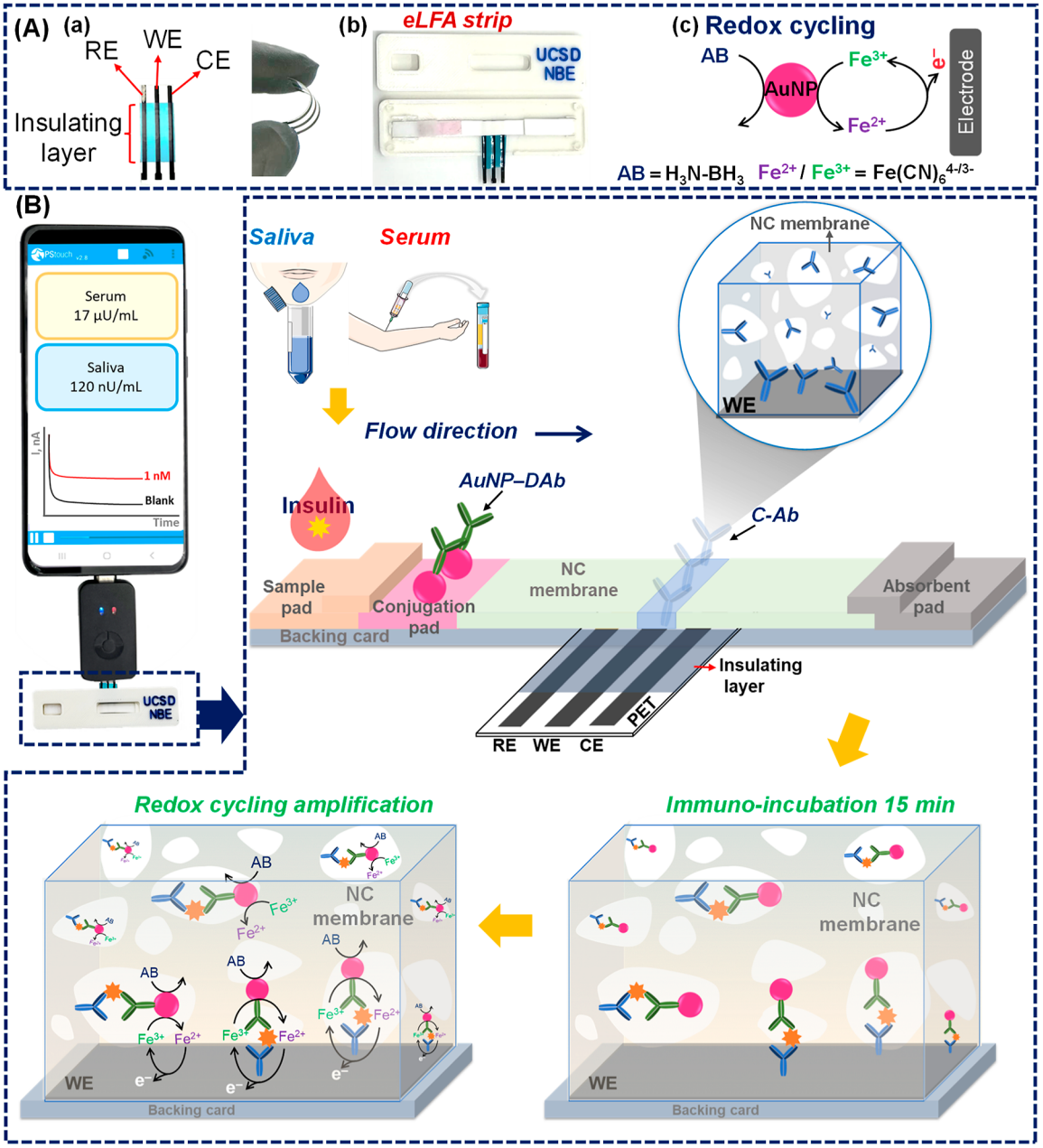

Figure 1. Redox cycling combined with electrochemical lateral flow immunoassay (eLFA) for insulin detection. (A) Components of the eLFA strip: (a) screen-printed electrodes on the PET substrate consisting of carbon working electrode (WE) and counter electrode (CE) and Ag/AgCl as a reference electrode (RE); a working area (5 mm^2) delimited with an insulating layer; (b) photo image of the developed eLFA strip and the homemade LFA case; and (c) schematic of nanocatalytic redox cycling employed to carry out the electrochemical transduction at eLFA. (B) Schematic of a simplified mobile insulin assay (eLFA strip) and possible electron-transferring reactions and signal amplification processes on an eLFA strip.

methods for trace-level insulin detection, such as immunoassays, are commonly time-consuming (due to the extended incubation and washing steps), expensive, and require skilled personnel and sophisticated equipment.[13] The complexity of such labor-intensive insulin immunoassays represents a major barrier to their future practical implementation as low-cost, scalable decentralized testing. Consequently, there are urgent needs for POC devices capable of rapid and sensitive insulin detection, empowering patients and healthcare providers with on-site monitoring capabilities.[13] By obviating labor-intensive steps, eLFA can greatly simplify point-of-care insulin measurements and thus minimize common large interpersonal and intrapersonal variations. While optical-based insulin LFAs have been previously studied, they have relatively limited sensitivity and detection limits.[17−19] eLFA represents a promising avenue for the development of user-friendly, cost-effective, and portable devices for insulin detection in a POC setting. However, owing to the extremely low (picomolar) concentrations of insulin in body fluids, new signal amplification schemes need to be developed for such portable and simple eLFA devices.

The most common amplification reactions employed in eLFA are (i) redox (oxidation or reduction) reactions of bound enzymes or nanocatalytic labels on either the nitro-

https://doi.org/10.1021/acssensors.3c01445
ACS Sens. 2023, 8, 3892−3901

cellulose (NC) membrane or the electrode surface (such as mediated reactions),[9,11] (ii) metal stripping or oxidizing the bounded metal nanoparticles with strong acidic solution,[20−24] and (iii) direct quantification of bounded electroactive species, which is linked to a detection probe.[25] Redox-cycling-based signal amplification has been widely used to lower the detection limits of electrochemical bioaffinity sensors.[26−32] The lower detection limits obtained by the redox cycling strategy reflect the greatly enhanced response as the signaling species contribute multiple times to the current signal. Such cycling consists of oxidation and reduction reactions and is achieved chemically, enzymatically, nanocatalytically, or electrochemically.[26] The metal stripping analysis with chemical dissolution enables high signal amplification while simultaneously offering high and irreproducible background levels. Moreover, using a strong acidic solution and applying a high oxidation potential at the electrode could damage the NC membrane and immunosensing layer on the sensing surface. The direct electron transfer of bound electroactive species is only possible within 1−2 nm from the electrode, and it is even more challenging to obtain a reproducible signal on the LFA platform. In electrochemical detection, the mass transfer of signaling species to the electrode surface limits the current signals because only a small volume of signaling species is consumed during analysis. Redox cycling, on the other hand, serves to amplify electrochemical signals by effectively regenerating the signaling species over a short period of time.

The development of a redox-cycling-integrated eLFA strip requires flexible conductive electrodes in the LFA platform and stable and rapidly dissolvable redox cycling components. Our eLFA strip consists of (i) a flexible screen-printed carbon electrode (SPCE) and (ii) stable redox cycling components such as ferro/ferricyanide ($[Fe(CN)_6]^{3-/4-}$, $Fe^{3+/2+}$), ammonia-borane ($H_3N{-}BH_3$, AB), and AuNP as the mediator, reductant, and catalytic label, respectively (Figure 1A). AB is a hydrogen storage material that is readily soluble in aqueous solutions.[33−35] Despite being a strong reducing agent, AB is stable in air and in aqueous solutions. In the presence of a nanocatalyst, AB readily undergoes catalytic hydrolysis, which can catalytically reduce nitro(so) arenes and organometallic mediators.[36,37] In the present study, the capture insulin antibody (C-Ab) was immobilized on the test line zone (both the NC membrane and carbon working electrode) and the AuNP-labeled detection insulin antibody (AuNP−DAb) was immobilized on the conjugate pad (Figure 1B). The specific insulin detection was facilitated by the flow of the target insulin sample through capillary action and simultaneous binding with AuNP−DAb and C-Ab to form a typical sandwich-type immunoassay on the eLFA platform. Such a developed insulin-sensing eLFA strip strategy can be easily coupled with smart phone-based AuNP-labeled detection insulin antibody (AuNP−DAb) mobile electrochemical analyzers. In the presence of target insulin, the bounded AuNP catalytically reduces Fe^{3+} with the support of AB. The resulting nanocatalytic reduction on both the NC membrane and the working electrode and the electrochemical oxidation of the catalytic product (Fe^{2+}) with redox cycling reactions are thus measured amperometrically at the carbon working electrode transducer surface (Figure 1B). The developed insulin eLFA sensor operation led to the ultrasensitive detection of insulin, as will be discussed in the following sections.

EXPERIMENTAL SECTION

Reagents and Solutions. Insulin, bovine serum albumin (BSA), sucrose, antimouse IgG produced in goat, horseradish peroxidase-labeled antimouse IgG produced in goat, IgG from mouse serum, gold nanoparticles (AuNP, 15 nm), l-ascorbic acid, uric acid, acetaminophen, 2-(*N*-morpholino)ethanesulfonic acid (MES), pyrenebutyric acid, 1-ethyl-3-(3-(dimethylamino)propyl) carbodiimide (EDC), *N*-hydroxysuccinimide (NHS), and phosphate buffer solution (PB, 1.0 M, pH 7.4) were obtained from Sigma-Aldrich. Insulin antibodies (10-2397 as capture antibodies (C-Ab) and 10-2396 as DAb) were purchased from Fitzgerald Industries International. Potassium ferricyanide (III) ($K_3[Fe(CN)_6]$) and Tween-20 were acquired from Fisher Scientific, and borane−ammonia complex ($H_3N{-}BH_3$, AB) from Tokyo Chemical Industry (TCI, Tokyo, Japan). Phosphate buffered saline (PBS, 4 mM, pH 7.4) was acquired from Gibco. TMB substrate was obtained from Neogen (Enhanced K-Blue TMB Substrate). Carbon and silver/silver chloride (Ag/AgCl) inks were obtained from Ercon Inc.

Electrochemical and colorimetric LFA strips were made by using backing cards (DCN Backing card) purchased from DCN Dx (60 mm × 300 mm), nitrocellulose membrane (UniSart CN 95) from Sartorius, and glass fiber diagnostic pad (GFDX203000) for sample and conjugate pads and cellulose fiber (CFSP001700) for adsorbent pad were all from EDM Millipore.

Phosphate buffer (PB, 10 mM, pH 7.4) was prepared by diluting 1.0 M PB buffer in deionized water. Phosphate buffer was supplemented with Tween 20 (PBT, 10 mM, pH 7.4, containing 0.05% Tween-20). Borate buffer (5 mM, pH 8.5) was prepared by dissolving sodium borate (borux) in deionized water and changing the pH with NaOH and HCl. Insulin stock solution was prepared in PBT containing 32 μM HCl, and it was further diluted in PBT. For IgG detection, mouse IgG was prepared in PBT.

Saliva samples from authors were collected using Sarstedt's Salivettes (Sarstedt, Nümbrecht, Germany). Swabs were chewed for 1 min, then placed into the Salivette's upper cavity and centrifuged immediately for 2 min at 1000*g* to obtain the available saliva for laboratory use. Human serum samples from 3 undefined males were acquired from BioreclamationIVT and used without any dilution.

Equipment and Instruments. SPCE used in the eLFA strips and conventional electrochemical immunoassays was printed by using a semiautomatic MMP-SPM printer (Speedline Technologies, Franklin, Massachusetts) to spread the carbon ink onto a poly(ethylene terephthalate) (PET) sheet, assisted by the use of a stainless-steel stencil as a template. While the working electrode (WE) and counter electrode (CE) were made of carbon ink, the reference electrode (RE) was made by applying a second layer of Ag/AgCl ink. After each printed layer, the homemade electrodes were baked in an oven at 80 °C for 10 min. Once the electrodes were printed, a 5 mm^2 sensing area was set up with an insulating layer.

All electrochemical measurements were performed at room temperature using an EmStat3 Blue potentiostat (PalmSens, The Netherlands) controlled by PSTrace software, version 5.9.

A catalytic reduction study of the Fe^{3+}/AuNP/AB system was carried out using a spectrophotometer (UV-2450) purchased from the Shimadzu Corporation.

Scanning electron microscopy (SEM) images were obtained by using a FEI Apero microscope.

AuNP−DAb Conjugate. A conjugate solution was prepared by incubating 10 μL of 1 mg/mL the detection antibody (antimouse IgG or antihuman insulin antibody) with 500 μL AuNP added drop by drop on a 1% (w/v) BSA-treated microcentrifuge tube. After constant and gentle stirring for 30 min, 100 μL of 0.6 or 1% BSA in 10 mM PB (for insulin or mouse IgG detection) was added with stirring for 5 min and centrifuged for 50 min at 10,000 rpm. After centrifugation, the supernatant was discarded, and the precipitate was suspended in 500 μL of borate buffer (5 mM, pH 8.5). The solution of the AuNP-DAb conjugate was stirred for 20 min and used directly without further dilution. SEM images of the AuNP-DAb conjugate in Figure

https://doi.org/10.1021/acssensors.3c01445
ACS Sens. 2023, 8, 3892−3901

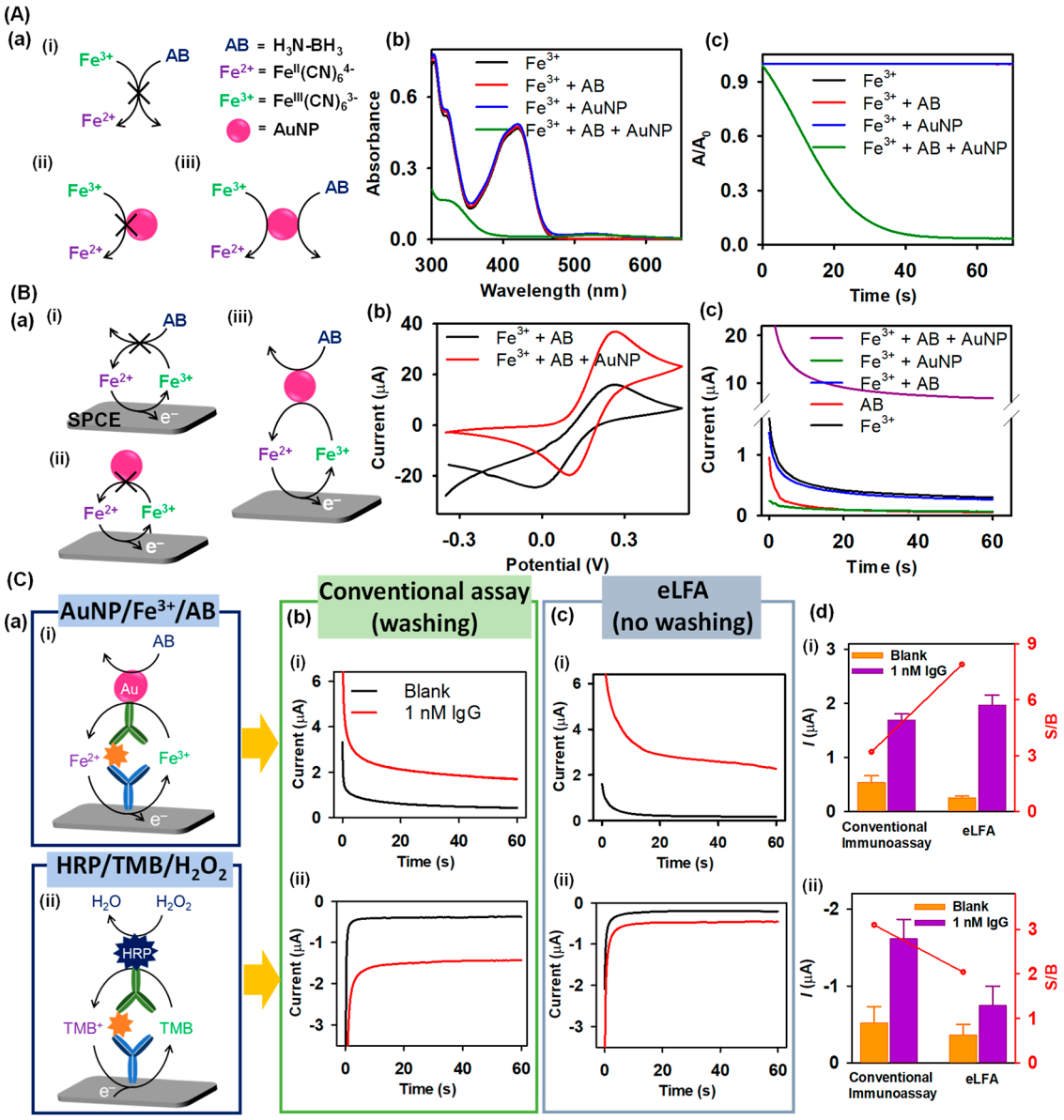

Figure 2. Activity of the Fe^{3+}/AuNP/AB redox system. (A) Catalytic reduction of $[Fe(CN)_6]^{3-}$ (Fe^{3+}) with AuNP and AB: (a) Schematic of catalytic reduction of Fe^{3+} (i) in the presence of AB; (ii) in the presence of AuNP; and (iii) in the presence of AuNP and AB. (b) UV/vis absorbance spectra for the catalytic reduction of Fe^{3+}. (c) Time-course spectra of absorbance vs time (at λ = 420 nm) for catalytic reduction of Fe^{3+} (the concentrations of Fe^{3+}, AuNP, and AB in PBS were 50 μM, 1 μg/mL, and 5.0 mM, respectively). (B) Nanocatalytic redox cycling of Fe^{3+} with AuNP and AB at SPCE: (a) Schematic of the redox cycling in the (i) absence of AuNP, (ii) absence of AB, and (iii) presence of Fe^{3+}, AuNP, and AB; (b) CVs recorded for Fe^{3+} and AB in the absence or presence of AuNP; and (c) amperometric response of Fe^{3+} and AB in the absence or presence of AuNP recorded at +0.3 V (the concentrations of Fe^{3+}, AuNP, and AB in PBS were 5.0 mM, 1 μg/mL, and 5.0 mM, respectively). (C) IgG detection: (a) Schematic of the immuno-reaction scheme using (i) Fe^{3+}/AuNP/AB or (ii) TMB/HRP/H_2O_2, (b,c) amperometric response of (b) a conventional one-step electrochemical immunoassay (washing) and (c) the new eLFA (no washing) for IgG detection 0 (black curve) and 1 nM (red curve) recorded at different potentials of (i) + 0.3 V (AuNP redox system) and (ii) −0.1 V (HRP redox system); and (d) recorded current comparison for three replicates of IgG detection at different conditions, with 0 (orange bars) and 1 nM IgG (purple bars).

S1 in Supporting Information confirm that AuNP in the conjugate was well dispersed and not aggregated.

eLFA and cLFA Strip Fabrication and Immunoassay Protocol. The preparation of the test strips for the electrochemical was divided into three sections: fabrication of the screen-printed electrodes, fabrication, and functionalization of the lateral flow strips.

The eLFA and cLFA strip dimensions are shown in Figure S2. The fabrication of the eLFA test strips was divided into three steps: First, the screen-printed electrode was placed on the backing card before the NC membrane (5 mm × 30 mm) was attached, and a 1 μL aliquot of the 0.5 mg mL^{-1} C-Ab (antimouse IgG or antihuman insulin antibody) was immobilized onto the working electrode zone to cover both the WE and NC membranes and incubated for 5 h at 4 °C. Meanwhile, a sample pad was prepared by soaking a glass fiber membrane (5 mm × 14 mm) in sample pad buffer (PBS supplemented with 2% BSA, 2% sucrose, and 0.1% Tween 20) and drying it for 25 min at 35 °C. A conjugate pad was prepared by dipping 50 μL of AuNP−DAb conjugate (or 1 μg/mL HRP-DAb for IgG detection) on a glass fiber membrane (5 mm × 12 mm) and drying it for 25 min at 35 °C. Then, the conjugate pad, sample pad, and absorbent pad (5 mm × 12 mm) were placed on a backing card with around 3 mm overlap between them [Figure 1A(b)]. 100 μL of insulin (or IgG)-containing sample was dropped on the sample pad, and it was allowed to flow for 15 min. For insulin-spiked human

https://doi.org/10.1021/acssensors.3c01445
ACS Sens. 2023, 8, 3892−3901

serum or saliva sample analysis, first, 50 μL of sample was dropped on the sample pad, and after 2 min, 50 μL of PBT was dropped and allowed to flow for 20 min. In the presence of insulin (or IgG), it binds simultaneously with AuNP−DAb on the conjugate pad and with the C-Ab on the working electrode zone to form a sandwich-type immunoassay on the eLFA platform. Electrochemical measurements (chronoamperometry at +0.3 V) were performed after dropping 15 μL of a mixture solution containing Fe^{3+}/AB (5.0 mM in PBS) into the working electrode zone. The detection is based on nanocatalytic redox cycling (Fe^{3+}/AuNP/AB), requiring 30 s for catalytic reduction on the NC membrane. The second scan of amperometric data was considered for the analysis, and the data were processed on SigmaPlot 14.0. Similarly, for enzymatic (TMB/HRP/H_2O_2) redox cycling, 15 μL of commercial TMB solution was dropped on the working electrode zone, and amperometric currents (at −0.1 V) were measured.

The fabrication of cLFA strips was the same as described for eLFA strips without placing the screen-printed electrode on the backing card and adding an additional control line (1 μL of 0.25 mg/mL mouse IgG) next to the test line (antimouse IgG) to capture the AuNP-DAb. Sample pad and conjugate pad conditions were the same as for eLFA. For IgG detection, images of the cLFA strips were acquired from an Apple iPhone 13, and test line intensities were analyzed using ImageJ software.

Conventional One-Step Electrochemical Immunoassay. A 5 μL aliquot of 20 mM of pyrenebutyric acid in 10 mM PB (pH 7.4) was drop-cast on the carbon WE surface and incubated for 2 h at room temperature in a humid chamber.[38,39] The electrodes were washed with PB and air-dried, and 5 μL of 25 mM MES buffer (pH 6.5) containing 400 mM EDC and 100 mM NHS was incubated for 35 min at room temperature to activate the carboxylate groups. After washing with PB, 5 μL of antimouse IgG (C-Ab, 100 μg/mL) was incubated for 45 min on the activated surface. Then, the electrodes were washed with PB and dried again, followed by the deactivation of unreacted carboxylate groups with 10 μL of 1% BSA prepared in PB for 30 min. Subsequently, 10 μL of a mixture solution containing 1 nM IgG and AuNP−DAb conjugate (or 1 μg/mL HRP-DAb) in 10 mM PBT was incubated for 15 min at room temperature, and after one-time washing with PB, amperometric responses of corresponding catalytic reactions were recorded with 15 μL of Fe^{3+}/AB (or TMB/H_2O_2) reagent solutions.

RESULTS AND DISCUSSION

Catalytic Activity of the Fe^{3+}/AuNP/AB Redox System. Initial efforts have been devoted to optimizing and characterizing the redox cycling strategy used for amplifying the eLFA sensor strip. Obtaining reproducible electrical signals is of prime importance in developing amplified electrochemical LFA systems. The electrochemical response of the newly developed eLFA platform depends on the rapid catalytic reduction of associated redox species (e.g., Fe^{3+}) with AuNP and AB and the selective redox cycling reactions on the transducer surface. Key strategies for selecting stable redox cycling components are (i) excellent self-stability of each component, such as the electron mediator ($Fe^{2+/3+}$), nanocatalyst (AuNP), and reductant (AB); (ii) direct reduction of Fe^{3+} with only AuNP or AB should be slow or not present; and (iii) rapid catalytic reduction of Fe^{3+} with both the AuNP and AB [Figure 2A(a)]. $Fe^{2+/3+}$ is a well-known stable electron mediator, and AuNP has been widely used as a signal tag in LFA systems. Similarly, AB is a stable reductant in an aqueous solution and undergoes catalytic hydrolysis only in the presence of a catalyst. To investigate the catalytic reduction of Fe^{3+}, we recorded the absorption spectra of Fe^{3+} in the absence and presence of associated redox species in phosphate buffer (10 mM phosphate buffer (PB), pH 7.4) [Figure 2A(b)]. Fe^{3+} shows an absorbance peak at 420 nm, whereas negligible absorbance was observed at this wavelength for AuNP and AB (Figure S3). The absorbance of Fe^{3+} did not change with either the presence of AuNP or AB but decreased significantly in the presence of both components [Figure 2A(b,c)]. It is clearly evident that Fe^{3+} was catalytically reduced to Fe^{2+} in the presence of AuNP and AB. The electrochemical behavior of the redox cycling components was examined in a PB solution to confirm the selective redox cycling at the bare carbon electrode (Figure 2B). In agreement with the UV absorption results, selective and high redox cycling currents were obtained by running cyclic voltammetry for Fe^{3+} with AuNP and AB [Figures 2B(b) and S4]. Additionally, the chronoamperometric data of all of the redox components were assessed at +0.3 V through the measurement of the nanocatalytic product (Fe^{2+}) [Figure 2B(c)]. In the presence of AuNP, Fe^{3+} ions were chemisorbed on the nanoparticle, leading to a lower current than free Fe^{3+}.[40] Lower anodic currents of Fe^{3+} in the presence of AB and high redox cycling currents of Fe^{3+} with AuNP and AB revealed that the nanocatalytic redox cycling described above is rapid and very selective. The ability of the developed nanocatalytic redox cycling to detect 1 nM IgG in PBS was compared with the standard TMB/HRP/H_2O_2 system employing two different configurations: (i) conventional electrochemical immunoassay, including a final washing step carried out on the surface of SPCEs and on the (ii) developed eLFA strip (Figure 2C). Both formats employed similar operational variables for IgG detection, e.g., the experimental parameters involved in sandwich formation and amperometric transduction, except for the additional washing required by the conventional electrochemical immunoassay. Figure 2C(a) illustrates the schematics of immunoassays with two different redox cycling systems: in the case of nanocatalytic redox cycling, AuNP served as the signal tag, with Fe^{3+}/AB acting as the mediator/substrate detection system, while electrochemical detection was performed by measuring Fe^{2+} oxidation currents. In standard enzymatic redox cycling, HRP was the signal tag, TMB/H_2O_2 served as the mediator/substrate, and detection was performed by measuring TMB reduction currents. In a one-step washing immunoassay, the capture antibody immobilization on the carbon working electrode involves covalent linkage to carboxylic acid groups of pyrenebutyric acid, and detection was performed through the incubation of 1 nM IgG and signal-tagged (AuNP or HRP) detection antibodies on the capture antibody-modified electrode surface, followed by amperometric detection of nanocatalytic (at +0.3 V) or enzymatic reaction (at −0.1 V) products. In the eLFA platform, the C-Ab was immobilized on both the NC membrane and the carbon working electrode, which was placed under the NC membrane. The target IgG was recognized by capillary flow from the sample pad to the conjugate pad, where it first binds to the signal-tagged DAb on the conjugation pad and then forms a sandwich complex with the C-Ab on the test line of the working electrode zone. The subsequent amperometric detection involves detecting the corresponding reaction products from the associated catalytic reaction of the signal tag. The amperometric current response in both formats is proportional to the target IgG concentration and is determined by the amount of captured signal tag. Figure 2C(b) displays a well-defined discrimination for blank vs one nM IgG (1 nM) was used in the conventional electrochemical immunosensor. While a large current response was observed for 1 nM IgG on the nanocatalytic eLFA platform {Figure

https://doi.org/10.1021/acssensors.3c01445
ACS Sens. 2023, 8, 3892−3901

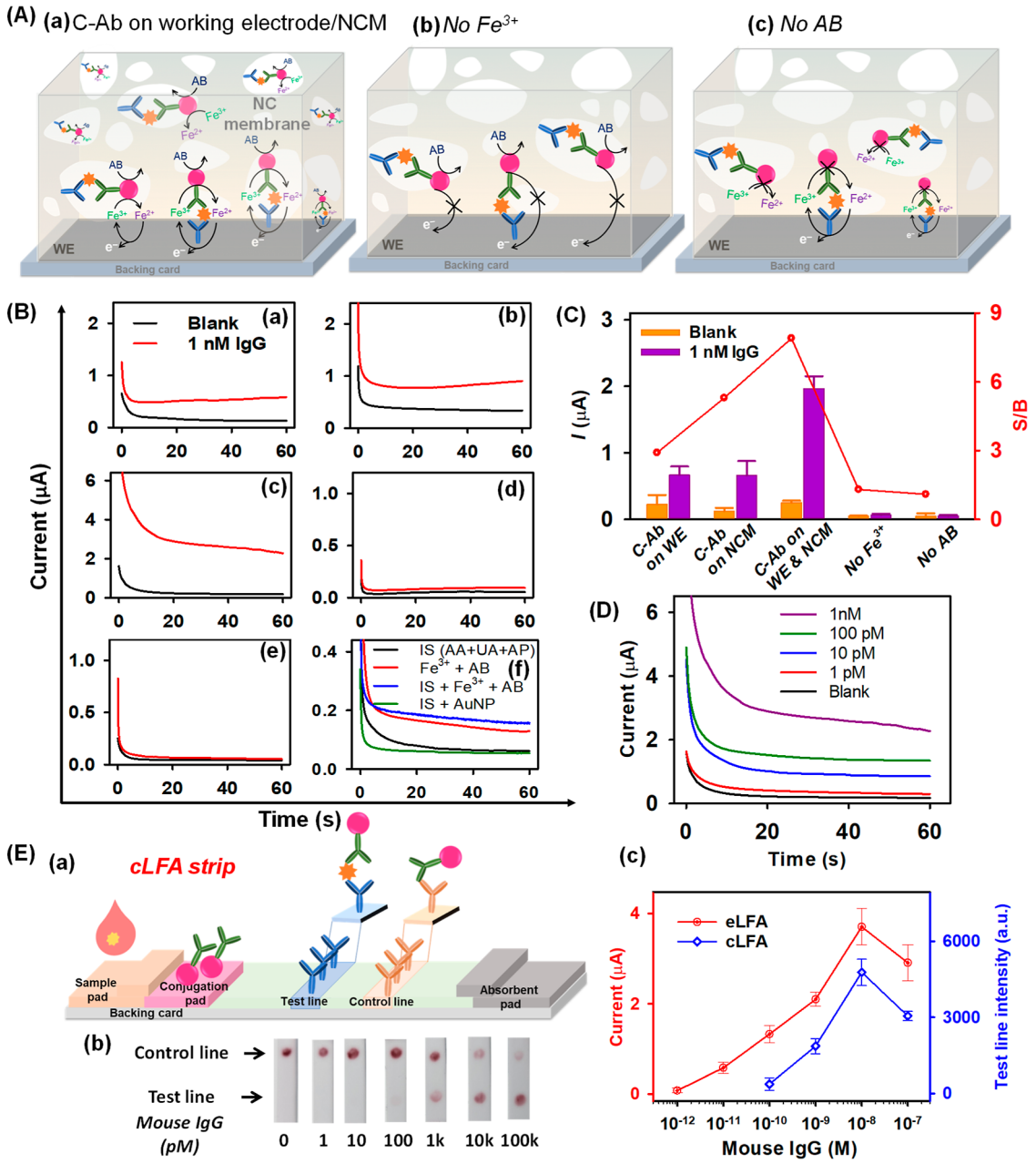

Figure 3. Feasibility study of the Fe^{3+}/AuNP/AB on eLFA and comparison of the analytical performance offered by eLFA vs cLFA. (A) Schematic of possible electron transfer reactions on eLFA in the presence of (a) Fe^{3+} and AB, (b) AB, and (c) Fe^{3+}. (B) Amperometric response (at +0.3 V) for 0 (black curves) and 1 nM (red curves) IgG at eLFA with different conditions: (a) capture antibody (C-Ab) present on the nitrocellulose membrane (NCM); (b) C-Ab present on the working electrode (WE); (c−e) C-Ab present on WE and NCM (c) Fe^{3+} and AB, (d) AB only, (e) Fe^{3+} only, and (f) influence of electroactive interfering species (IS) such as 50 μM ascorbic acid (AA), uric acid (UA), and acetaminophen (AP) in the analyte sample at eLFA (5.0 mM Fe^{3+} and/or 5.0 mM AB in PBS). (C) Comparison of the current response for three replicates of IgG detection at different conditions (a-e of Figure 3B), with 0 (orange bars) and 1 nM IgG (purple bars). (D) Amperometric response of the eLFA strip to increasing IgG concentrations from 0 to 1 nM in PBT. (E) (a) Schematic of the developed cLFA, (b) representative photo images of cLFA strips for IgG concentrations ranging from 0 to 100 nM, and (c) corresponding calibration curves of eLFA and cLFA (using the ImageJ program) for different IgG concentrations.

2C[c(i)]}, the enzymatic eLFA system did not exhibit a significant response to 1 nM IgG {Figure 2C[c(ii)]}. As seen in the bar graph in Figure 2C(d), among all the conditions, the nanocatalytic eLFA platform displays a high signal-to-background (S/B) ratio as well as a distinct signal difference between the blank and 1 nM IgG solutions. Such a comparison reveals that the eLFA platform with Fe^{3+}/AuNP/AB redox cycling enables better sensitivity than the commercial TMB/HRP/H_2O_2 redox cycling.

Sensitivity of the Redox Cycling-Amplified eLFA vs cLFA. The sensitivity of the eLFA strip directly depends on the effective accumulation of target analytes at the test line zone and then their conversion into measurable events on the transduction surface. The analyte accumulation and signal transduction on the LFA strip were controlled by the resulting immunocomplex on the test line through simultaneous binding of the analyte with AuNP−DAb and C-Ab. To examine this, IgG detection was performed by loading C-Ab only on the WE

https://doi.org/10.1021/acssensors.3c01445
ACS Sens. 2023, 8, 3892−3901

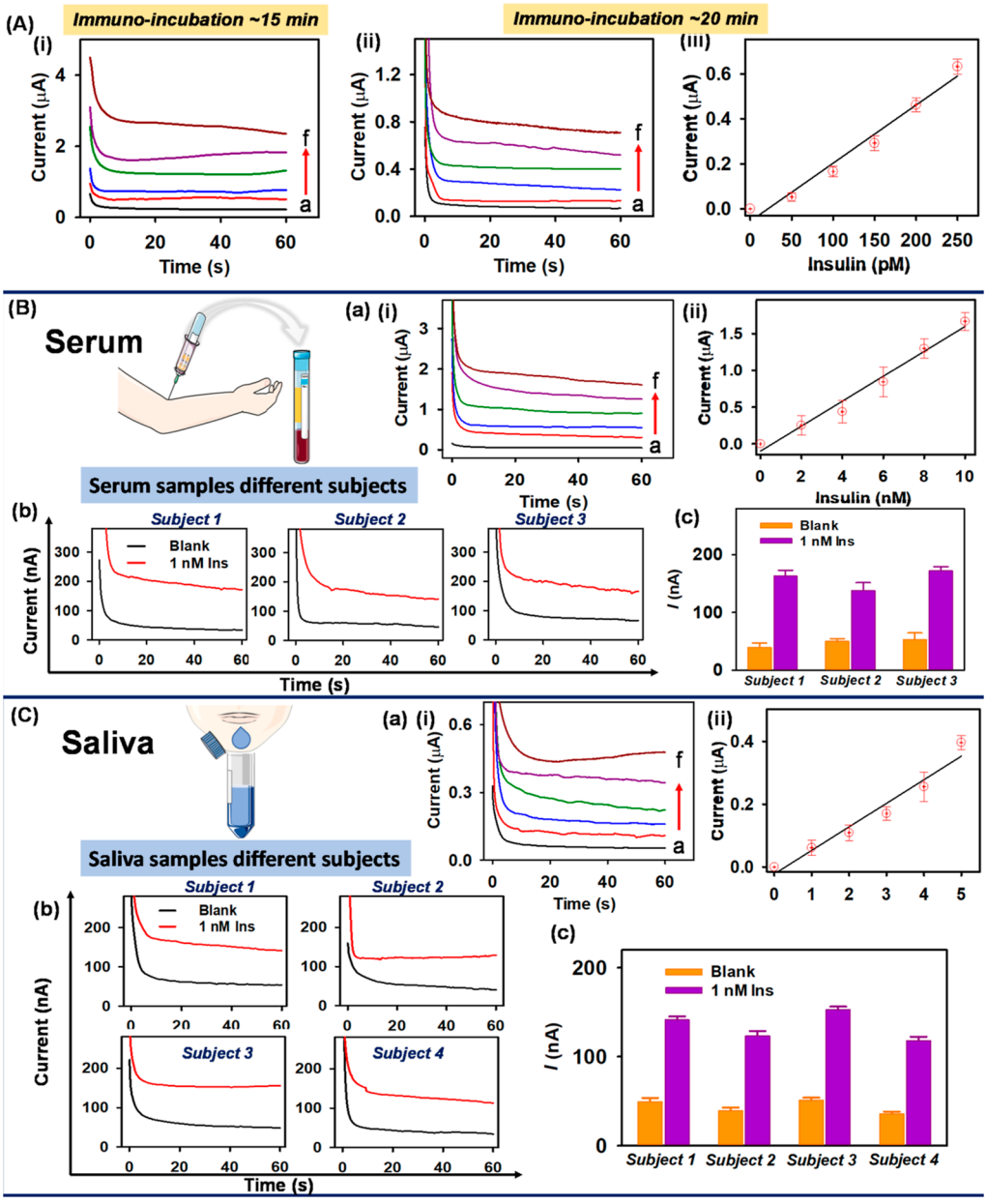

Figure 4. Electrochemical sensing performance of an eLFA strip for insulin detection. (A) Amperometric response of the eLFA strip for (i) 15 min incubation time for successive 250 pM insulin additions from 0 (a) to 1250 pM (f), (ii) 20 min incubation time for successive 50 pM insulin additions from 0 (a) to 250 pM (f), and (iii) corresponding calibration curve. Sensing performance of an eLFA strip in (B) human serum (a) (i) amperometric response of eLFA strip to increasing concentration of insulin from 0 (a) to 10 nM (f) in 2 nM steps; (ii) corresponding calibration curve, (b) eLFA performance in 1 nM insulin spiked human serum samples of three different subjects, and (c) amperometric current comparison for three replicates of three different human subjects, and (C) real human saliva (a) (i) amperometric response of eLFA strip to 1 nM increasing concentration of insulin from 0 (a) to 6 nM (f), (ii) corresponding calibration curve, (b) eLFA performance in 1 nM insulin spiked real human saliva samples of four different human subjects, and (c) amperometric current comparison for three replicates of four different human subjects.

surface or the NC membrane or on both the WE surface and the NC membrane. More IgG is expected to be accumulated on the NC membrane due to the large number of C-Ab on the capillary pores than on the transducer surface (Figures 3A and S5). When C-Ab is present only on the NC membrane, more catalytic product (Fe^{2+}) is accumulated through the nanocatalytic reduction, and electrochemical signals are generated from Fe^{2+} oxidation at the WE. In contrast, with C-Ab on the WE, less Fe^{2+} is generated, and the redox cycling reactions are responsible for the electrochemical signals (Figure S5). Importantly, C-Ab on both the WE and NC membranes affords a high amperometric signal with the contribution of nanocatalytic reduction on the NC membrane and redox cycling reactions on the transducer surface, which hold higher sensitivity than the other two conditions [Figure 3B(a–c)]. The reproducibility of the amperometric signals was assessed by measuring the response for the blank and 1 nM IgG solutions using three different eLFA strips fabricated using the same protocol (Figures 3C and S6). Moreover, a significant discrimination between the amperometric responses measured for blank and 1 nM IgG was observed only when the electrochemical measurements were performed in the presence of the mixture containing Fe^{3+} and AB, with negligible signals being measured using a single component (AB or Fe^{3+})

https://doi.org/10.1021/acssensors.3c01445
ACS Sens. 2023, 8, 3892−3901

[Figure 3B(d,e)]. After the C-Ab immobilizing type was selected for the eLFA strip, the parameters involved in the immunorecognition and the signal transduction components were systematically optimized (Figure S7). The optimum values for C-Ab concentration and sample pad components (sucrose and BSA) were found to be 500 μg/mL, sucrose (2%), and BSA (2%). In the case of redox cycling components such as Fe^{3+} and AB, concentrations were 5 mM. Upon establishing eLFA components, it was important to assess the interference of electroactive constituents (IS: ascorbic acid, uric acid, and acetaminophen) on the eLFA test strip as well as with redox cycling components by means of IS content on the developed eLFA test strip individually as well as with Fe^{3+}/AB and AuNP separately. As shown in Figure 3B(f), low amperometric currents are observed at +0.3 V, resulting in negligible contributions of IS due to sample flow with capillary action on the LFA platform. The analytical performance of the eLFA strip was further interrogated by measuring electrochemical currents for wide-ranging concentrations of IgG from 0 to 1 nM. As displayed in Figure 3D, well-defined amperometric signals are obtained for each increment. A limit of detection (LOD) for IgG in 10 mM PB of 2 pM can be estimated based on the calibration plot of Figure 3E(c) (Table S1 in the Supporting Information).

On the other hand, the sensitivity of the nanocatalytic redox cycling combined eLFA strip was compared with the conventional colorimetric LFA strip (cLFA) in Figure 3E. The naked-eye visible color signals, which are produced by the plasmonic activity of AuNP, were obtained on either the test or control line of the test strip. The color intensities at the test line increased as the concentration of IgG did, and vice versa at the control line [Figure 3E(b)]. The color intensities of the test line on the cLFA strips were quantified using ImageJ software, and the amperometric responses were measured using the developed eLFA (Figures 3D and S8). The resulting signals for increasing concentrations of IgG revealed a higher sensitivity achieved with the strategy, which is able to detect 100-fold lower concentrations than the colorimetric methodology [Figure 3E(c) and Table S1]. The developed eLFA system opens up a new opportunity by just integrating nanocatalytic redox cycling on lateral-flow systems to quickly and easily quantify a wide range of biomolecules.

Electrochemical Sensing Performance of an eLFA Strip for Insulin Detection. The optimized eLFA platform was applied to insulin detection using a similar detection principle as for IgG. The analytical performance of the insulin eLFA strip was evaluated in buffer medium (10 mM PB, pH 7.4) with increasing insulin concentrations from 0 to 1250 pM [Figure 4A(i)]. The current signals were well-defined for each pM increment, indicating that insulin binds simultaneously with AuNP−DAb on the conjugate pad and is captured with C-Ab on the working electrode zone. A linear response was observed in the calibration curve (Figure S9), and the calculated LOD is 74 pM for insulin. However, upon extending detection time to 20 min, the immunosensor can achieve a lower and narrower linear detection range of 0−250 pM, enabling precise measurements of even lower concentrations [Figure 4A(ii,iii)]. A LOD of 12 pM was obtained for 20 min of incubation, lower than that achieved by incubating for 15 min (Table S2). The developed eLFA could detect pM insulin levels at a wider concentration range than the existing cLFA.[17−19] These results support the feasibility of the eLFA strip for insulin detection with the same sensitivity that was achieved for IgG. The components of the sample matrixes can greatly affect the detection performance, and the capability to detect insulin in body fluids without requiring any treatment can significantly affect the clinical screening. In this sense, decreasing the amount of BSA in the sample pad enables better sensitivity for insulin in undiluted serum (Figure S10). As shown in Figure 4B(a), the undiluted serum samples were spiked with different concentrations of insulin from 0 to 10 nM, and distinct signal increments were observed for increasing insulin concentrations. We also obtained a calibration plot for insulin-spiked serum with its corresponding LOD of 460 pM (Table S3). Moreover, the reducibility of our biosensor was proved by measuring insulin-spiked human serum samples (collected from 3 different subjects), and all the samples exhibited a clearly defined response toward 1 nM insulin [Figure 4B(b,c)]. In a similar manner, the saliva samples were spiked with insulin to achieve a 1 nM increment in concentration.

The sensor exhibited good detection performance, showing a linear range of 0−5 nM, with an LOD of 690 pM [Figure 4D(a) and Table S3]. Furthermore, the measured current intensities show very limited error among the saliva of the four different subjects, further illustrating the reproducibility of the eLFA operation [Figure 4C(b,c)]. Although the blood and saliva samples demonstrated lower sensitivity compared to buffer solution due to matrix effects and biofouling on the transducer surface, the eLFA still displayed an attractive biosensing performance to effectively quantify insulin in different liquid biopsies collected with noninvasive or minimally invasive extraction processes.

CONCLUSIONS

In this work, we have demonstrated the first example of nanocatalytic redox cycling combined with eLFA for the sensitive detection of insulin in serum and saliva samples. Such decentralized insulin detection relies on the capillary flow of insulin through the series of sequential components on the LFA platform and simultaneous binding with AuNP−DAb on the conjugate pad and C-Ab on the NC membrane and the working electrode. Hence, by dramatically reducing the assay time, complexity, and costs, such eLFA facilitates POC insulin measurements. The nanocatalytic reduction on the NC membrane and redox cycling reactions on the carbon working electrode were responsible for the resulting electrochemical signals. The redox cycling amplification strategy on the eLFA platform displayed higher sensitivity than the conventional enzymatic redox cycling system and the colorimetric detection strategy. Distinct amperometric signals with corresponding analyte concentrations, reproducible results, discrimination against electroactive constituents, and favorable analytical performance in complex clinical samples demonstrate the feasibility of redox-amplified eLFA. However, new eLFA strips offer easy self-testing of insulin at home and in remote settings in connection to a miniaturized and portable potentiostat. Further efforts are needed toward faster testing, extensive large-scale clinical validation, and critical evaluation with many human specimens. Such a simple, user-friendly, highly sensitive biodevice, integrating redox cycling with commercial LFA kits, represents an attractive analytical tool for decentralized monitoring of other important trace-level disease-relevant biomarkers.

https://doi.org/10.1021/acssensors.3c01445
ACS Sens. 2023, 8, 3892−3901

■ ASSOCIATED CONTENT

Supporting Information

The Supporting Information is available free of charge at https://pubs.acs.org/doi/10.1021/acssensors.3c01445.

SEM images of AuNP−DAb, cLFA, and eLFA strip dimensions and additional eLFA optimization results and analytical characteristics data tables (PDF)

■ AUTHOR INFORMATION

Corresponding Author

Joseph Wang − *Department of Nanoengineering, University of California San Diego, La Jolla, California 92093, United States;* orcid.org/0000-0002-4921-9674; Email: josephwang@ucsd.edu

Authors

Ponnusamy Nandhakumar − *Department of Nanoengineering, University of California San Diego, La Jolla, California 92093, United States*

Cristina Muñoz San Martín − *Department of Nanoengineering, University of California San Diego, La Jolla, California 92093, United States; Departamento de Química Analítica, Universidad Complutense, E-28040 Madrid, Spain*

Beatriz Arévalo − *Department of Nanoengineering, University of California San Diego, La Jolla, California 92093, United States; Departamento de Química Analítica, Universidad Complutense, E-28040 Madrid, Spain*

Shichao Ding − *Department of Nanoengineering, University of California San Diego, La Jolla, California 92093, United States;* orcid.org/0000-0003-3795-306X

Mahika Lunker − *Department of Nanoengineering, University of California San Diego, La Jolla, California 92093, United States*

Eva Vargas − *Department of Nanoengineering, University of California San Diego, La Jolla, California 92093, United States*

Omeed Djassemi − *Department of Nanoengineering, University of California San Diego, La Jolla, California 92093, United States*

Susana Campuzano − *Departamento de Química Analítica, Universidad Complutense, E-28040 Madrid, Spain;* orcid.org/0000-0002-9928-6613

Complete contact information is available at: https://pubs.acs.org/10.1021/acssensors.3c01445

Author Contributions

[§]P.N., C.M.S.M., B.A., and S.D. contributed equally.

Notes

The authors declare no competing financial interest.

■ ACKNOWLEDGMENTS

This work was supported by the UCSD Center of Wearable Sensors. C.M.-S.M. and B.A. acknowledge predoctoral contracts from the Universidad Complutense de Madrid and the Spanish Ministerio de Ciencia, Innovación y Universidades, respectively.

■ REFERENCES

(1) Rink, S.; Baeumner, A. J. Progression of Paper-Based Point-of-Care Testing toward Being an Indispensable Diagnostic Tool in Future Healthcare. *Anal. Chem.* **2023**, *95* (3), 1785−1793.

(2) Sena-Torralba, A.; Álvarez-Diduk, R.; Parolo, C.; Piper, A.; Merkoçi, A. Toward Next Generation Lateral Flow Assays: Integration of Nanomaterials. *Chem. Rev.* **2022**, *122* (18), 14881−14910.

(3) Parolo, C.; Sena-Torralba, A.; Bergua, J. F.; Calucho, E.; Fuentes-Chust, C.; Hu, L.; Rivas, L.; Álvarez-Diduk, R.; Nguyen, E. P.; Cinti, S.; Quesada-González, D.; Merkoçi, A. Tutorial: Design and Fabrication of Nanoparticle-Based Lateral-Flow Immunoassays. *Nat. Protoc.* **2020**, *15* (12), 3788−3816.

(4) Parolo, C.; de la Escosura-Muñiz, A.; Merkoçi, A. Enhanced Lateral Flow Immunoassay Using Gold Nanoparticles Loaded with Enzymes. *Biosens. Bioelectron.* **2013**, *40* (1), 412−416.

(5) Loynachan, C. N.; Thomas, M. R.; Gray, E. R.; Richards, D. A.; Kim, J.; Miller, B. S.; Brookes, J. C.; Agarwal, S.; Chudasama, V.; McKendry, R. A.; Stevens, M. M. Platinum Nanocatalyst Amplification: Redefining the Gold Standard for Lateral Flow Immunoassays with Ultrabroad Dynamic Range. *ACS Nano* **2018**, *12* (1), 279−288.

(6) Liu, Y.; Zhan, L.; Qin, Z.; Sackrison, J.; Bischof, J. C. Ultrasensitive and Highly Specific Lateral Flow Assays for Point-of-Care Diagnosis. *ACS Nano* **2021**, *15* (3), 3593−3611.

(7) Wei, Z.; Luciano, K.; Xia, X. Catalytic Gold-Iridium Nanoparticles as Labels for Sensitive Colorimetric Lateral Flow Assay. *ACS Nano* **2022**, *16* (12), 21609−21617.

(8) Gupta, R.; Gupta, P.; Wang, S.; Melnykov, A.; Jiang, Q.; Seth, A.; Wang, Z.; Morrissey, J. J.; George, I.; Gandra, S.; Sinha, P.; Storch, G. A.; Parikh, B. A.; Genin, G. M.; Singamaneni, S. Ultrasensitive Lateral-Flow Assays via Plasmonically Active Antibody-Conjugated Fluorescent Nanoparticles. *Nat. Biomed. Eng.* **2023**.

(9) Kiba, Y.; Otani, Y.; Yasukawa, T.; Mizutani, F. Electrochemical Detection of Redox Species Flowing in a Nitrocellulose Membrane and Application to Quantitative Immunochromatography. *Electrochim. Acta* **2012**, *81*, 14−19.

(10) Cheng, J.; Yang, G.; Guo, J.; Liu, S.; Guo, J. Integrated Electrochemical Lateral Flow Immunoassays (ELFIAs): Recent Advances. *Analyst* **2022**, *147* (4), 554−570.

(11) Akanda, M. R.; Joung, H. A.; Tamilavan, V.; Park, S.; Kim, S.; Hyun, M. H.; Kim, M. G.; Yang, H. An Interference-Free and Rapid Electrochemical Lateral-Flow Immunoassay for One-Step Ultrasensitive Detection with Serum. *Analyst* **2014**, *139* (6), 1420−1425.

(12) Lian, K.; Feng, H.; Liu, S.; Wang, K.; Liu, Q.; Deng, L.; Wang, G.; Chen, Y.; Liu, G. Insulin Quantification towards Early Diagnosis of Prediabetes/Diabetes. *Biosens. Bioelectron.* **2022**, *203*, 114029.

(13) Vargas, E.; Nandhakumar, P.; Ding, S.; Saha, T.; Wang, J. Insulin Detection in Diabetes Mellitus: Challenges and New Prospects. *Nat. Rev. Endocrinol.* **2023**, *19*, 487−495.

(14) American Diabetes Association. Insulin Administration. *Diabetes Care* **2004**, *27* (suppl_1), s106−s107.

(15) Shen, Y.; Prinyawiwatkul, W.; Xu, Z. Insulin: A Review of Analytical Methods. *Analyst* **2019**, *144* (14), 4139−4148.

(16) Brink, S. J. Insulin Past, Present, and Future: 100 Years from Leonard Thompson. *Diabetology* **2022**, *3* (1), 117−158.

(17) Oyama, Y.; Osaki, T.; Kamiya, K.; Kawano, R.; Honjoh, T.; Shibata, H.; Ide, T.; Takeuchi, S. A Glass Fiber Sheet-Based Electroosmotic Lateral Flow Immunoassay for Point-of-Care Testing. *Lab Chip* **2012**, *12* (24), 5155.

(18) Berryhill, E. H.; Urbina, N. S.; Marton, S.; Vernau, W.; Alonso, F. H. Validation and Method Comparison for a Point-of-Care Lateral Flow Assay Measuring Equine Whole Blood Insulin Concentrations. *J. Vet. Diagn. Invest.* **2023**, *35* (2), 124−131.

(19) Jekarl, D. W.; Choi, H.; Kim, E. S.; Lee, S.; Park, H.-I.; Kim, M.; Kim, Y. Analytical Evaluation and Clinical Application of Insulin and C-Peptide by a Whole Blood, Lateral Flow, Point of Care (POC) Assay System. *Scand. J. Clin. Lab. Investig.* **2019**, *79* (5), 347−353.

(20) Lu, F.; Wang, K. H.; Lin, Y. Rapid, Quantitative and Sensitive Immunochromatographic Assay Based on Stripping Voltammetric Detection of a Metal Ion Label. *Analyst* **2005**, *130* (11), 1513−1517.

(21) Liu, G.; Lin, Y. Y.; Wang, J.; Wu, H.; Wai, C. M.; Lin, Y. Disposable Electrochemical Immunosensor Diagnosis Device Based

on Nanoparticle Probe and Immunochromatographic Strip. *Anal. Chem.* **2007**, *79* (20), 7644−7653.
(22) Srisomwat, C.; Yakoh, A.; Chuaypen, N.; Tangkijvanich, P.; Vilaivan, T.; Chailapakul, O. Amplification-Free DNA Sensor for the One-Step Detection of the Hepatitis B Virus Using an Automated Paper-Based Lateral Flow Electrochemical Device. *Anal. Chem.* **2021**, *93* (5), 2879−2887.
(23) Lin, Y. Y.; Wang, J.; Liu, G.; Wu, H.; Wai, C. M.; Lin, Y. A Nanoparticle Label/Immunochromatographic Electrochemical Biosensor for Rapid and Sensitive Detection of Prostate-Specific Antigen. *Biosens. Bioelectron.* **2008**, *23* (11), 1659−1665.
(24) Ariño, C.; Banks, C. E.; Bobrowski, A.; Crapnell, R. D.; Economou, A.; Królicka, A.; Pérez-Ràfols, C.; Soulis, D.; Wang, J. Electrochemical Stripping Analysis. *Nat. Rev. Methods Primers* **2022**, *2* (1), 62.
(25) Deenin, W.; Yakoh, A.; Kreangkaiwal, C.; Chailapakul, O.; Patarakul, K.; Chaiyo, S. Integrated Lateral Flow Electrochemical Strip for Leptospirosis Diagnosis. *Anal. Chem.* **2022**, *94* (5), 2554−2560.
(26) Yang, H. Enzyme-Based Ultrasensitive Electrochemical Biosensors. *Curr. Opin. Chem. Biol.* **2012**, *16* (3−4), 422−428.
(27) Wang, J. *Analytical Electrochemistry*, 4th ed.; John Wiley and Sons: New York, 2023.
(28) Walter, A.; Wu, J.; Flechsig, G.-U.; Haake, D. A.; Wang, J. Redox Cycling Amplified Electrochemical Detection of DNA Hybridization: Application to Pathogen E. Coli Bacterial RNA. *Anal. Chim. Acta* **2011**, *689* (1), 29−33.
(29) Ronkainen-Matsuno, N. J.; Thomas, J. H.; Halsall, H. B.; Heineman, W. R. Electrochemical Immunoassay Moving into the Fast Lane. *TrAC, Trends Anal. Chem.* **2002**, *21* (4), 213−225.
(30) Akanda, M. R.; Ju, H. An Integrated Redox Cycling for Electrochemical Enzymatic Signal Enhancement. *Anal. Chem.* **2017**, *89* (24), 13480−13486.
(31) Akanda, M. R.; Ju, H. A Tyrosinase-Responsive Nonenzymatic Redox Cycling for Amplified Electrochemical Immunosensing of Protein. *Anal. Chem.* **2016**, *88* (19), 9856−9861.
(32) Akanda, M. R.; Ju, H. Ferritin-Triggered Redox Cycling for Highly Sensitive Electrochemical Immunosensing of Protein. *Anal. Chem.* **2018**, *90* (13), 8028−8034.
(33) Demirci, U. B. Ammonia Borane: An Extensively Studied, Though Not Yet Implemented, Hydrogen Carrier. *Energies* **2020**, *13* (12), 3071.
(34) Gil-San-Millan, R.; Grau-Atienza, A.; Johnson, D. T.; Rico-Francés, S.; Serrano, E.; Linares, N.; García-Martínez, J. Improving Hydrogen Production from the Hydrolysis of Ammonia Borane by Using Multifunctional Catalysts. *Int. J. Hydrogen Energy* **2018**, *43*, 17100.
(35) Stephens, F. H.; Pons, V.; Tom Baker, R. Ammonia-Borane: The Hydrogen Source Par Excellence? *Dalton Trans.* **2007**, *2* (25), 2613−2626.
(36) Nandhakumar, P.; Kim, B.; Lee, N.-S.; Yoon, Y. H.; Lee, K.; Yang, H. Nitrosoreductase-Like Nanocatalyst for Ultrasensitive and Stable Biosensing. *Anal. Chem.* **2018**, *90* (1), 807−813.
(37) Nandhakumar, P.; Bhatia, A.; Lee, N. S.; Yoon, Y. H.; Yang, H. Rapid Nanocatalytic Reaction Using Antibody-Conjugated Gold Nanoparticles for Simple and Sensitive Detection of Parathyroid Hormone. *Int. J. Biol. Macromol.* **2023**, *241* (February), 124574.
(38) Hinnemo, M.; Zhao, J.; Ahlberg, P.; Hägglund, C.; Djurberg, V.; Scheicher, R. H.; Zhang, S.-L.; Zhang, Z.-B. On Monolayer Formation of Pyrenebutyric Acid on Graphene. *Langmuir* **2017**, *33* (15), 3588−3593.
(39) Torrente-Rodríguez, R. M.; Lukas, H.; Tu, J.; Min, J.; Yang, Y.; Xu, C.; Rossiter, H. B.; Gao, W. SARS-CoV-2 RapidPlex: A Graphene-Based Multiplexed Telemedicine Platform for Rapid and Low-Cost COVID-19 Diagnosis and Monitoring. *Matter* **2020**, *3* (6), 1981−1998.
(40) Qi, Y.; Brasiliense, V.; Ueltschi, T. W.; Park, J. E.; Wasielewski, M. R.; Schatz, G. C.; Van Duyne, R. P. Plasmon-Driven Chemistry in Ferri-/Ferrocyanide Gold Nanoparticle Oligomers: A SERS Study. *J. Am. Chem. Soc.* **2020**, *142* (30), 13120−13129.

https://doi.org/10.1021/acssensors.3c01445
ACS Sens. 2023, 8, 3892−3901